Creep-cyclic plasticity and damage assessment of an SS304 weldolet

Manu Puliyaneth and Haofeng Chen*

Department of Mechanical & Aerospace Engineering, University of Strathclyde, Glasgow, G1 1XJ, UK

**Corresponding author email: haofeng.chen@strath.ac.uk*

Abstract: Creep-fatigue and creep-ratcheting life assessment of an SS304 weldolet considering full creep-cyclic plasticity interaction is investigated using the extended Direct Steady Cycle Analysis (eDSCA) within the Linear Matching Method Framework (LMMF). The creep behaviour is modelled using the Norton relationship, which is modified by the Arrhenius rule to account for the temperature variation within the weldolet. The introduction of a creep dwell increases the reverse plasticity resulting from the creep relaxation. This leads to both creep-fatigue and creep-ratcheting damage mechanisms at different regions within the weldment. For thermal load dominated loading combinations, creep ratcheting due to both cyclically enhanced creep and creep enhanced plasticity are observed based on the dwell period. The effect of dwell period, load and temperature on the creep-fatigue and creep-ratcheting interaction of a weldolet are presented. The simultaneous presence of various damage mechanisms at different locations within the weldment highlights the importance and requirement of the proposed creep-cyclic plasticity investigations at weld locations.

Keywords: Creep - Cyclic Plasticity Interaction; Creep-Fatigue; Creep-Ratcheting; LMM; Weld

1. Introduction

The introduction of a dwell period at high operating temperature introduces creep effect on the structure. The presence of welds further complicates the structural response. Considering both the economic and safety aspects, the life assessment of welds under creep-fatigue loading is a critical issue in reactors [1]. Creep-fatigue damage evaluation has seen significant progress over the years with the development and further refining of standard codes such as ASME [2] and R5 [3], nevertheless, it is still observed in industries as the actual problems are far more complex than the well-controlled research environment in a lab [4]. With the development in the field of renewable energy, power plants are expected to accommodate flexible modes of operation which will have frequent start-ups and shut-downs, thereby subjecting the piping system to severe loading conditions.The introduction of flexible operations within the power plants increases the susceptibility of creep-fatigue and thermo-mechanical fatigue damage at the weldments.

This is a peer-reviewed, accepted author manuscript of the following article: Puliyaneth, M., & Chen, H. (2021). Creep-cyclic plasticity and damage assessment of an SS304 weldolet. Journal of Pressure Vessel Technology, Transactions of the ASME. https://doi.org/10.1115/1.4051931

Similar to creep-fatigue, creep-ratcheting is another dangerous and complex mechanism that occurs when inelastic strain accumulates within the structure due to either dominant creep or reverse plasticity strains. As the inelastic strain is not compensated in a cycle, creep-ratcheting produces an open hysteresis loop at steady state [5, 6]. For weldments, different regions may experience different damage mechanisms and it is important to identify each of them to assess the safe life of the component.

The work presented within this study aims at investigating the creep-fatigue and creep-ratcheting damage of a welded T-piece header-branch connection (weldolet) under a constant mechanical load and a cyclic temperature load, considering full interaction between creep and cyclic plasticity via 3D Finite Element Analysis (FEA) using the extended Direct Steady Cycle Analysis (eDSCA) within the Linear Matching Method Framework (LMMF) [7]. The impact of applied load level and creep dwell on the failure mechanism and location are investigated. The effect of two internal pressures are investigated, one which is in the range of a typical operating pressure while the other is significantly higher.

2. Creep-cyclic plasticity interaction

The response of a structure under cyclic loading changes significantly with the introduction of a creep dwell. A schematic representation of the different possible creep-cyclic plasticity responses is presented in [6, 8]. If creep is introduced for load levels within the elastic limit, a hysteresis loop similar to Figure 1 (a) will be observed. On increasing the load levels to within the shakedown region but well below the shakedown limit, the structural response is similar to Figure 1 (b). For both these scenarios, at steady state, the inelastic strain accumulation that results in ratcheting is due to the creep effect. If the load levels are further increased and plasticity occurs during unloading, the structural response hysteresis will be either one from Figure 1 (c) to Figure 1 (f). For scenarios corresponding to Figure 1 (c) and Figure 1 (d), the reverse plasticity compensates for the creep strain and any plastic strain during loading. This results in a larger but closed hysteresis loop signifying creep-fatigue damage. If the creep strain and any plastic strain are not compensated by the reverse plasticity or vice versa, an open hysteresis loop will be observed resulting in creep-ratcheting. If the open-loop (Figure 1 (e)) is driven due to the enhanced creep strain, the creep ratcheting process is termed as “cyclically enhanced creep”. For instance, consider the scenario where the structure is subjected to a large dwell time, in such cases it is possible that a very large creep strain is accumulated during the dwell period and the plastic strain during unloading cannot compensate for it. If very large stress relaxation occurs during the dwell period leading to an insignificant creep strain accumulation and large plastic strain is accumulated during unloading, the resultant hysteresis will be similar to the one shown in Figure 1 (f). The open hysteresis loop here is driven by the reverse plasticity strain. This phenomenon is known as “creep enhanced plasticity”.

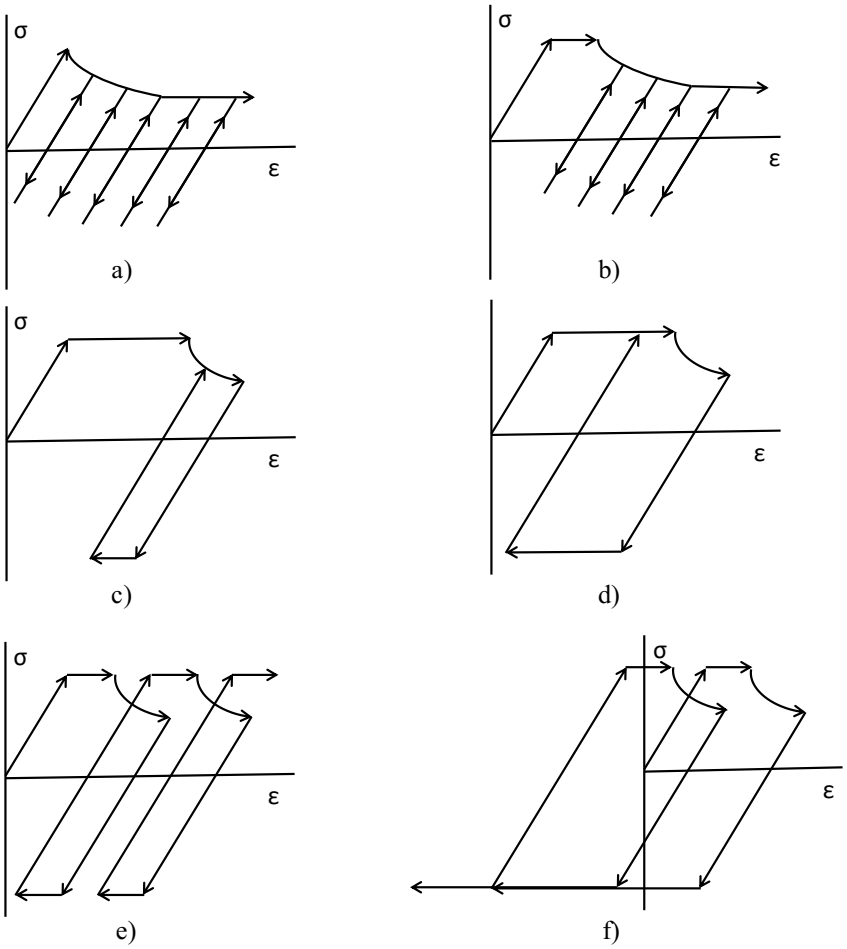

Figure 1 Variation in the cyclic plasticity responses with creep dwell a) elastic response [6, 8]; b) elastic shakedown [6, 8]; c) creep-cyclic plasticity due to creep enhanced reversed plasticity [6, 8]; d) creep-cyclic plasticity shakedown due to creep enhanced plasticity [6, 8]; e) creep-ratcheting due to cyclically enhanced creep; and f) creep-ratcheting due to creep enhanced plasticity.

3. The creep-fatigue damage assessment procedure

The creep-fatigue damage assessment procedures for both the ASME and R5 has certain limitations, for example, the creep and plasticity interaction is not completely accounted for, and the start of dwell stress is calculated by very conservative methods [6]. Whereas, the LMM eDSCA considers the full creep-cyclic plasticity interaction. The LMM eDSCA allows the calculation of key parameters such as loading and unloading stress, the loading and unloading strains (elastic and plastic), the creep stain, the end of dwell stress and the elastic follow up factor. They help in the easy identification of the extend of creep-cyclic plasticity interaction and the damage calculations. The general methodology adopted in this study for evaluating the creep-fatigue damage of the component is illustrated in Figure 2 [9]. It consists of four main steps.

1. Estimation of saturated hysteresis loop using the Linear Matching Method (LMM).
2. Estimation of fatigue damage using Strain-Life (E–N) diagrams.
3. Estimation of creep damage using Time Fraction (TF) rule.
4. Estimation of total damage using the interaction diagram.

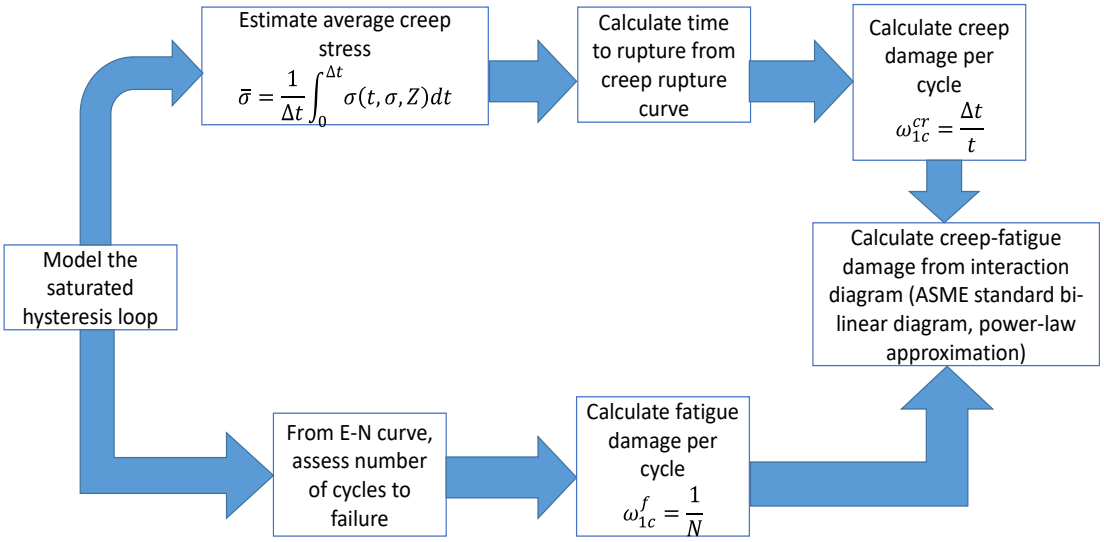

Figure 2 Flow-chart for the general creep-fatigue evaluation procedure [9].

Step 1: Estimation of saturated hysteresis loop using eDSCA within LMM framework

There are various direct methods which can be used in conjunction with FEA for modelling and analysis of structures under high-temperature and mechanical load. The LMM has been developed for limit analysis [10], shakedown analysis [11], ratchet analysis [12, 13], and recently to include steady-state cyclic behaviour with full creep-cyclic plasticity interaction [7, 14]. The LMM ensures that both equilibrium and compatibility are satisfied at all stages. The numerical procedure detailing the evaluation of creep strain using eDSCA has been explained previously in [7]. Hence only a concise version of the numerical procedure is presented here. A minimization process $I\left(\dot{\varepsilon}_{ij}^{c}\right) = \sum_{l=1}^{L} I^{l}$ was proposed by Chen *et. al* in [15] to calculate the steady-state cyclic response of a body subjected to an arbitrary cyclic load history, where L is the total number of loading instances and $\dot{\varepsilon}_{ij}^{c}$ is the kinematic admissible strain rate. For the defined minimization function, an incremental form is proposed:

$$I^{l}\left(\Delta\varepsilon_{ij}^{l}\right) = \int_{V} \left\{\sigma_{ij}^{l}\Delta\varepsilon_{ij}^{l} - \left[\hat{\sigma}_{ij}^{l}(t_l) + \rho_{ij}^{l}(t_l)\right]\Delta\varepsilon_{ij}^{l}\right\}dV \tag{1}$$

where $\Delta\varepsilon_{ij}^{l}$ is the strain increment and $\rho_{ij}^{l}(t_l)$ is the residual stress, which is the sum of the previous

changing residual stress field increment $\Delta\rho_{ij}(t_l)$ and the constant part of the changing residual stress $\bar{\rho}_{ij}$. In an iterative manner, $\Delta\varepsilon_{ij}^{l}$ is calculated by minimizing the function in Equation (1). Assuming l is the number of load instances considered, and k is the number of sub-cycles required to reach convergence. The residual stresses and the inelastic strains are calculated based on the elastic stress and the previous accumulated residual stresses at each increment. For the load instance t_l during the loading cycle, $\Delta\varepsilon_{ij,k+1}(t_l)$ is calculated by:

$$\Delta\varepsilon_{ij,k+1}(t_l)' = \frac{1}{2\bar{\mu}(t_l)}\left[\hat{\sigma}_{ij}(t_l) + \rho_{ij,k+1}(t_{l-1}) + \Delta\rho_{ij,k+1}(t_l)\right]' \tag{2}$$

where $\bar{\mu}$ is the iterative shear modulus, $\hat{\sigma}_{ij}$ is the associated elastic solution, $\rho_{ij,k+1}(t_{l-1})$ is the prior changing residual stress history and $\Delta\rho_{ij,k+1}(t_l)$ is the current changing residual stress associated with that inelastic strain increment. When creep is considered for the load cases, the equivalent creep strain increment is calculated by:

$$\Delta\bar{\varepsilon}^{c} = \frac{B(n-1)\Delta t^{m+1}(\bar{\sigma}_s - \bar{\sigma}_c)}{\left(\frac{1}{\bar{\sigma}_c^{n-1}} - \frac{1}{\bar{\sigma}_s^{n-1}}\right)(m+1)} \tag{3}$$

$$\bar{\sigma}_c = \left(\frac{\dot{\bar{\varepsilon}}^{F}}{B\Delta t^{m}}\right)^{\frac{1}{n}} \tag{4}$$

$$\dot{\bar{\varepsilon}}^{F} = \frac{\Delta\bar{\varepsilon}^{c}}{\Delta t}\frac{(m+1)}{(n-1)}\frac{\bar{\sigma}_c^{n}}{(\bar{\sigma}_s - \bar{\sigma}_c)}\left(\frac{1}{\bar{\sigma}_c^{n-1}} - \frac{1}{\bar{\sigma}_s^{n-1}}\right) \tag{5}$$

where B, m and n are the creep constants of the material, $\bar{\sigma}_c$ represents the creep flow stress, and it is defined as the sum of the start of dwell stress, $\bar{\sigma}_s$ and the residual stress $\Delta\rho_{ij,k+1}(t_l)$ during the dwell period. Equation (4) is used to calculate $\bar{\sigma}_c$ and Equation (5) is in-turn used to calculate $\dot{\bar{\varepsilon}}^{F}$, which is the creep strain rate. The next step involves calculating the residual stress and iterative shear modulus at each increment using the linear solutions previously calculated. The below equation is used for it:

$$\bar{\mu}_{k+1}(x,t_l) = \bar{\mu}_k(x,t_l)\frac{\sigma_y^R(x,t_l)_k}{\bar{\sigma}\left(\hat{\sigma}_{ij}(x,t_l) + \rho_{ij}^{r}(x,t_l)_k\right)} \tag{6}$$

where $\bar{\mu}_{k+1}(x,t_l)$ is the iterative shear modulus at the sub-cycle k for l^{th} load instance. $\sigma_y^R(x,t_l)_k$ is either the iterative von-Mises yield stress for the material model considered at load instance t_l or the

creep flow stress $\bar{\sigma}_c$. $\rho_{ij}^r(x, t_l)$ is the sum of the constant residual stress field and all previous changing residual stresses at load instance t_l. The procedure briefly detailed in this section helps in determining all the parameters required for the estimation of the saturated hysteresis loop.

Step 2: Estimation of fatigue damage

The number of cycles to Low Cycle Fatigue (LCF) damage is related to the total strain range. The total strain range at steady state is obtained from the previous step. Based on the available experimental data, a quadratic polynomial, cubic polynomial, or a power-law function is obtained which relates the number of cycles to failure and the total strain range. The obtained expression is used within the LMM subroutine for post-processing and obtaining the fatigue damage per cycle. Fatigue damage accumulated per cycle calculated as:

$$d_f = \frac{1}{N^{\circ}(\Delta\varepsilon_{tot})} \tag{7}$$

where d_f is the fatigue damage per cycle and N° is the number of cycles to crack initiation due to pure fatigue corresponding to the total strain range, $\Delta\varepsilon_{tot}$.

Step 3: Estimation of creep damage

Considering that the dwell times used for the study is over 720 hours (1 month), it is safe to assume that the secondary creep strain will be the most prominent. Hence, Norton creep law, is used to compute the creep strain, the uniaxial form of which is given by:

$$\dot{\varepsilon}^{cr} = A\sigma^n \tag{8}$$

where $\dot{\varepsilon}^{cr}$ is the creep strain rate, σ is the applied stress in MPa; A and n are the creep constants. In order to implement the non-isothermal effects, the creep constant A is modified using the Arrhenius law as:

$$A = A^{\star} exp\left(\frac{-Q_{act}}{R_{gas}T}\right) \tag{9}$$

where Q_{act} is the activation energy in kJ/mol; R_{gas} is the global gas constant $kJ\ /\ mol\ /\ K$; T is the temperature in Kelvin and $A^{\star}$ is the frequency factor. The TF rule is used for the creep-damage assessment. The time to creep rupture t^{rup} is described by the reverse power-law mentioned below:

$$t^{rup} = B^{TF}\sigma_{avg}^{-k^{TF}} \tag{10}$$

with B^{TF} and k^{TF} are the creep constants and σ_{avg} is the average stress over the dwell period Δt which is calculated as:

$$\sigma_{avg}(\Delta t, \sigma_1, Z) = \frac{1}{\Delta t}\int_0^{\Delta t} \sigma(\Delta t, \sigma_{cs}, Z)dt \tag{11}$$

where Z is the elastic follow up factor and σ_{cs} is the stress at the beginning of dwell period. Both of them are obtained from step 1. The creep damage per cycle is then defined as:

$$d_c = \frac{\Delta t}{t^{rup}(\sigma_{avg})} \tag{12}$$

Step 4: Creep-fatigue interaction

The next step is to calculate the total number of cycles under creep-fatigue interaction using the creep-fatigue damage interaction diagram. Creep damage per cycle, d_c and fatigue damage per cycle, d_f are calculated in the previous steps. This is used to calculate $\mathrm{D_c} = N^{\Delta}d_c$ and $\mathrm{D_f} = N^{\Delta}d_f$, where $\mathrm{D_c}$ and $\mathrm{D_f}$ are the creep and fatigue damage accumulated by the structure until failure and N^{Δ} is the total number of cycles under creep-fatigue interaction. As per continuum damage mechanics, it is assumed that

$$\mathrm{D_f} + \mathrm{D_c} \leq 1 \tag{13}$$

The detailed procedure, approximations, and solutions to calculate N^{Δ} is provided in [14, 16], hence, only equations relevant to this study is provided below. N^{Δ} is calculated by solving Equation (14)

$$aN^{\Delta 2} - bN^{\Delta} + 1 = 0 \tag{14}$$

where the root is

$$N^{\Delta} = \left(-b - \sqrt{b^2 - 4ac}\right)/2a \tag{15}$$

with

$$a = [d_c]^2 + \left[\omega_{1c}^{f}\right]^2 + d_c\,.\,d_f \tag{16}$$

$$b = -2d_c - 2d_f \tag{17}$$

4. Weldolet geometry, FE model and material properties

An SS304 weldolet consisting of two weldments, as shown in Figure 3, is used within the study, one connects the weldolet to the main pipe while the second weldment connects the weldolet to the branch pipe. The weldolet geometry corresponds to one typically found in a steam header in a combined cycle gas turbine plant, similar to the study in [17, 18]. Due to the symmetry condition of the model, a quarter of the weldolet is used for the simulation. A symmetric boundary condition is applied on the x-y and y-z plane of the elbow, and plane end condition is applied on both the free ends of the pipe. Quadratic hexahedral elements of type C3D20R [19] is used for structural analysis and quadratic hexahedral elements of type DC3D20 [19] is used for heat transfer analysis. Both the end of the main pipe and branch pipe are constrained to expand in-plane. The total no of elements is 6, 495 with the mesh finely refined near the weldment which is the weakest area.

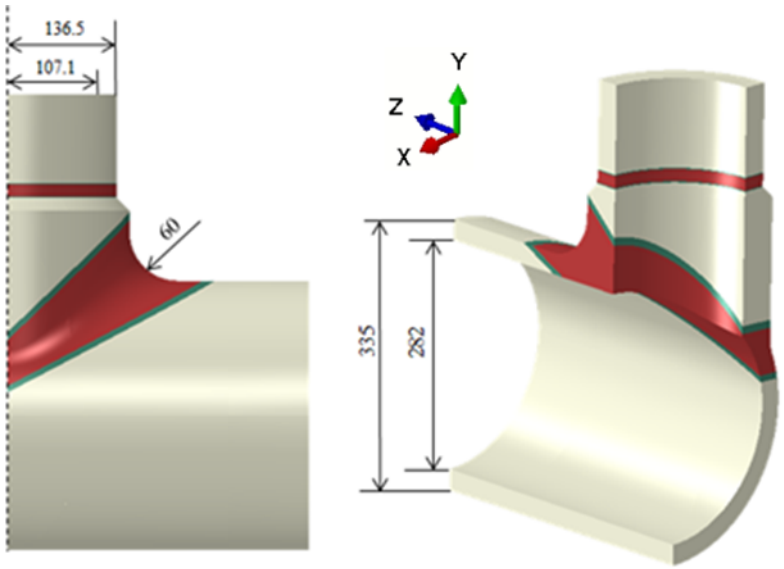

Figure 3 3D weldolet model with key dimensions (in mm) [17, 18].

The weldment comprises of three zones; 1) the parent material (PM), 2) the weld metal (WM) and 3) the heat-affected zone (HAZ). It is considered that all the three zones exhibit elastic-perfectly plastic (EPP) material properties and that they satisfy the von Mises yield condition. The LMM is a direct method that calculates the steady state response of a structure subjected to cyclic loading using the cyclic stress-strain curve, where the cyclic stress-strain curve has already considered cyclic hardening or softening effects of material. Hence, when they are used within the LMM calculations, the results inherently will be influenced by the hardening/softening behavior of the material. Hence, the accuracy

of the analysis greatly depends on the material properties of the three different zones considered in the weldment. It is quite challenging to obtain all of them from a single source; hence, from the available literature, a general database is generated and used for the analysis. A. Hossein *et al.* [20, 21] in their study have presented a range of mechanical properties, generated creep constitutive parameters, and temperature and stress-dependent creep properties for the SS304 PM, HAZ, and WM, which is used within this study. The EN curve for the PM at room temperature is initially generated from the NIMS database and then modified for higher temperatures and the WM. The material is considered to have a thermal conductivity of 43 $Wm^{-1}K^{-1}$ and a Poisson's ratio of 0.3. Certain reasonable modification and assumptions are made to account for any unavailable material property. When material properties for the WM and HAZ are available only for a certain temperature, they are assumed to follow a trend similar to that of the PM and are extrapolated/interpolated. The complete set of material properties and the Strain-life Curve (E-N curve) used are presented in Table 1 to Table 5 and Figure 4 respectively. The residual stress in the pipe due to welding is assumed zero due to the Post Weld Heat Treatment (PWHT).

Table 1 Temperature-dependent yield stress.

Temp ℃	25	680	700	720
$\sigma_y^{PM}\ (MPa)$	426	319	305	290
$\sigma_y^{HAZ}\ (MPa)$	151	113	108	98
$\sigma_y^{WM}\ (MPa)$	298	223	213	194

Table 2 Temperature-dependent Young's modulus.

Temp ℃	25	680	700	720
$E_y\ (MPa)$	179500	145200	116200	116000

Table 3 Co-efficient of thermal expansion.

Material Zone	PM	HAZ	WM
$\alpha(\text{x } 10^{-6}℃)$	1.8	1.9	2.1

Table 4 Norton creep strain parameters.

Material Zone	$A^{\star}(MPa^{-n}h^{-1})$	$Q(J/mol\,K)$	n
PM	6.0121 x 10^{-5}	2.6 x 10^5	5.72
HAZ	92.448 x 10^{-3}	2.6 x 10^5	4.76
WM	97.838 x 10^{-3}	2.6 x 10^5	4.59

Table 5 Creep rupture properties.

	B^{TF}			k^{TF}
Temp ℃	580	600	620	
PM	$5.37\times10^{+18}$	$2.31\times10^{+18}$	$1.03\times10^{+18}$	5.77
HAZ	$1.92\times10^{+15}$	$8.39\times10^{+14}$	$3.81\times10^{+14}$	4.70
WM	$1.58\times10^{+15}$	$6.91\times10^{+14}$	$3.14\times10^{+14}$	4.50

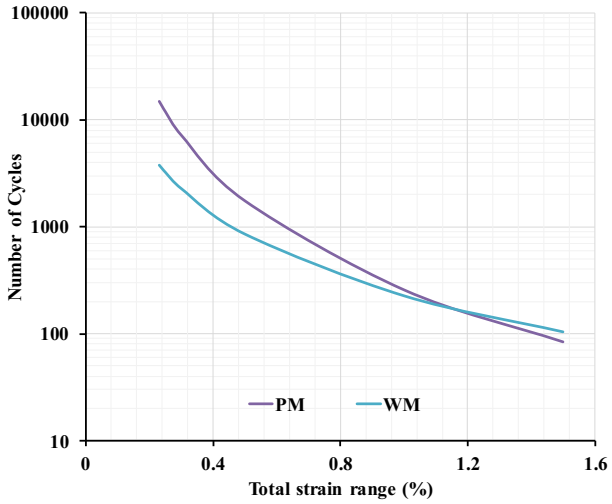

Figure 4 Strain-life Curve (E-N Curve) at 600 ℃.

For baseline studies, an internal pressure of 17 MPa, which is in range with the typical pipe pressure in a power plant, and a cyclic thermal load with a fluctuation of 40 ℃ across the thickness of the weldolet is considered. The inner temperature is 580 ℃ and the outer temperature is 620 ℃. The effects of higher pressure and temperature are investigated by carrying out additional studies by increasing the internal pressure to 25 MPa and the thermal load by a factor of 1.2.

5. Results and discussions

Linear elastic analysis is performed for the weldolet subjected to mechanical load and thermal load to understand their individual loading effects. The resultant von-Mises elastic stress contours for the mechanical load at ambient temperature, and the thermal load are illustrated in Figure 5. From the contours, it can be inferred that the magnitude of equivalent stress under the thermal load is larger than that under the mechanical load, but within a comparable scale. The stress concentration due to the mechanical load is enhanced by the geometric feature whereas it is the material property that influences the concentration of thermal load.

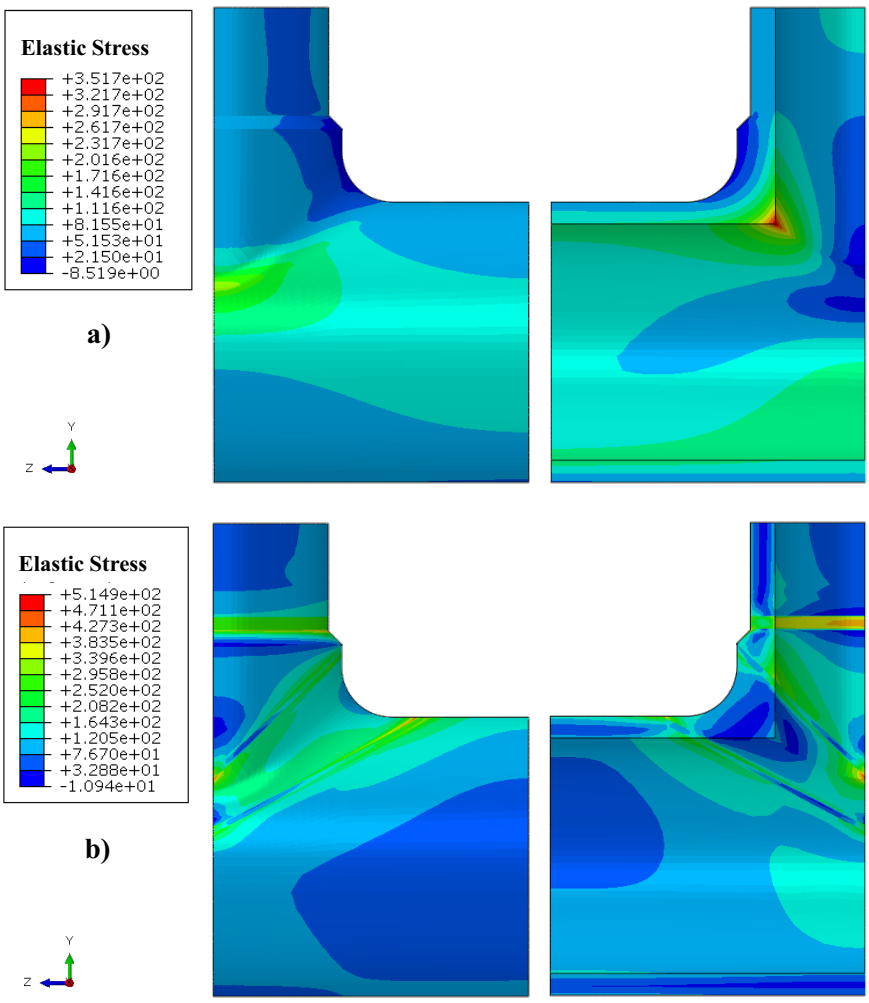

Figure 5 von-Mises elastic stress solutions a) mechanical load at ambient temperature; b) thermal load

5.1 Cyclic plasticity behaviour

As an initial step, before imposing a creep dwell, high-temperature fatigue analysis is carried out. Figure 6 presents the contours of total strain range and fatigue damage per cycle at steady-state. It is evident that there is substantial damage accumulation at both the weldment regions. But the most critical region is at the HAZ-WM intersection at the inner side of the pipe where the weldolet connects to the header pipe, where the strain accumulation is enhanced by the geometric irregularity.

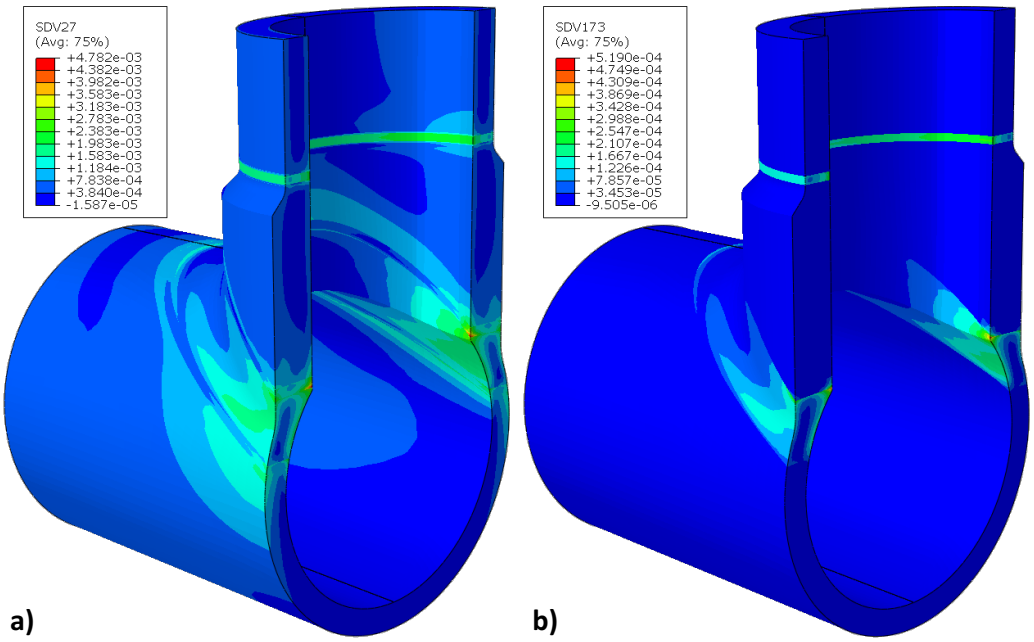

Figure 6 Contours for a) Total strain range and b) Fatigue damage per cycle.

The open hysteresis loop in Figure 7 indicates that the component experiences a small accumulation of plastic strain with each cycle, indicating ratcheting. The yield stress at the higher temperature is considerably lower than at the room temperature. This results in larger plastic strain accumulation during loading that is not compensated equally during the unloading sequence. It should be noted that the net plastic strain accumulation per cycle is very small, hence though present, ratcheting is not considered to be the major damage mechanism in this case whereas LCF damage is prominent. The cycles to LCF failure is estimated to a total of 4295 cycles. It is to be noted that as the calculation does not consider any hardening of the material, the results for the pure fatigue case are conservative.

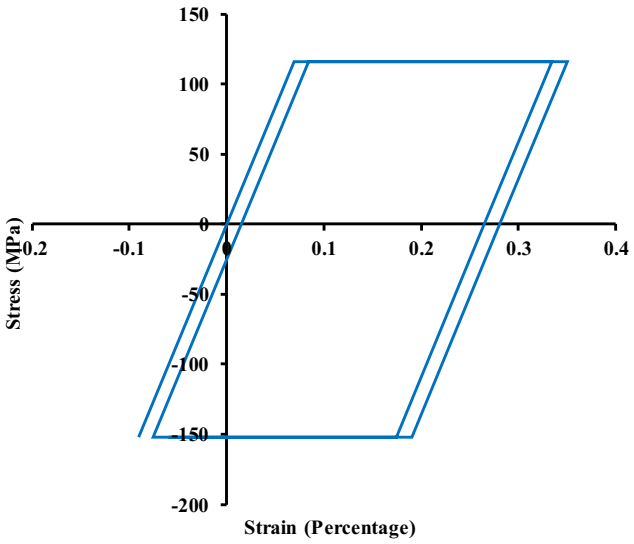

Figure 7 Steady-state hysteresis loop for pure fatigue case.

5.2 Creep-Cyclic plasticity

As introduced in Section 3, the temperature-dependent function for the creep strain can be expressed using the Arrhenius law, $A = A^{\star} \exp\left(\frac{-Q_{act}}{R_{gas}T}\right)$. Since a thermal gradient is present across the thickness of the weldolet, the Norton law is combined with the Arrhenius law and used for the creep strain calculations. Figure 8 shows the isothermal thermal field applied and the creep parameter thus obtained.

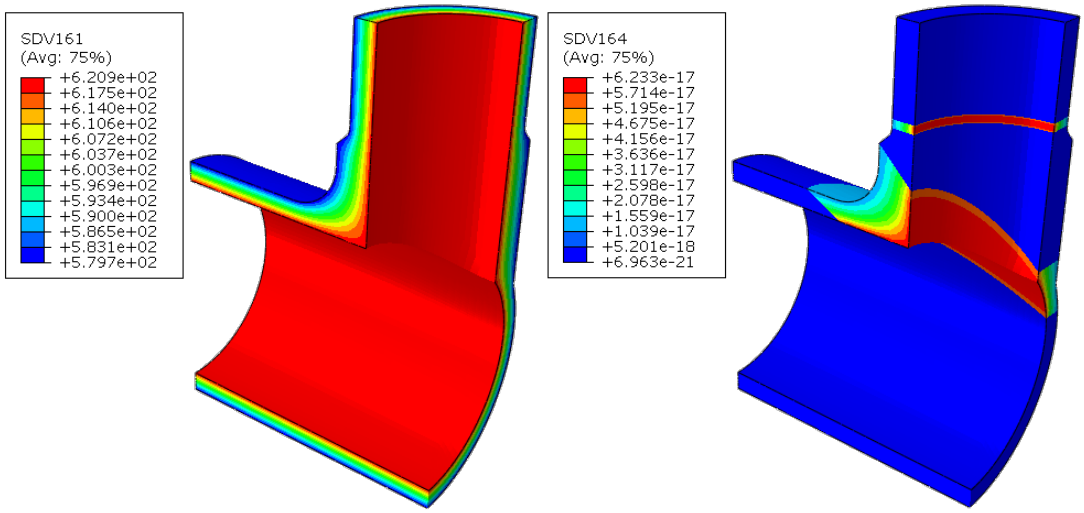

Figure 8 a) Thermal load applied; b) Temperature-dependent creep parameter.

The effect of dwell time on the end of creep and unloading stresses are presented in Figure 9. Generally, for a single material component, the stress reduces during creep dwell, but for a multi-material such as a weldment, the stress re-distribution during a creep dwell is not always straightforward. Some regions within the structure can experience stress relaxation while the other regions experience an increase in stress. For the weldolet considered here, with an increase in the dwell time, the stress near the weldment regions decreases while it increases at certain regions in the PM. The higher stress relaxation will lead to a larger strain accumulation during unloading. This will lead to larger hysteresis loops as shown in the subsequent sections.

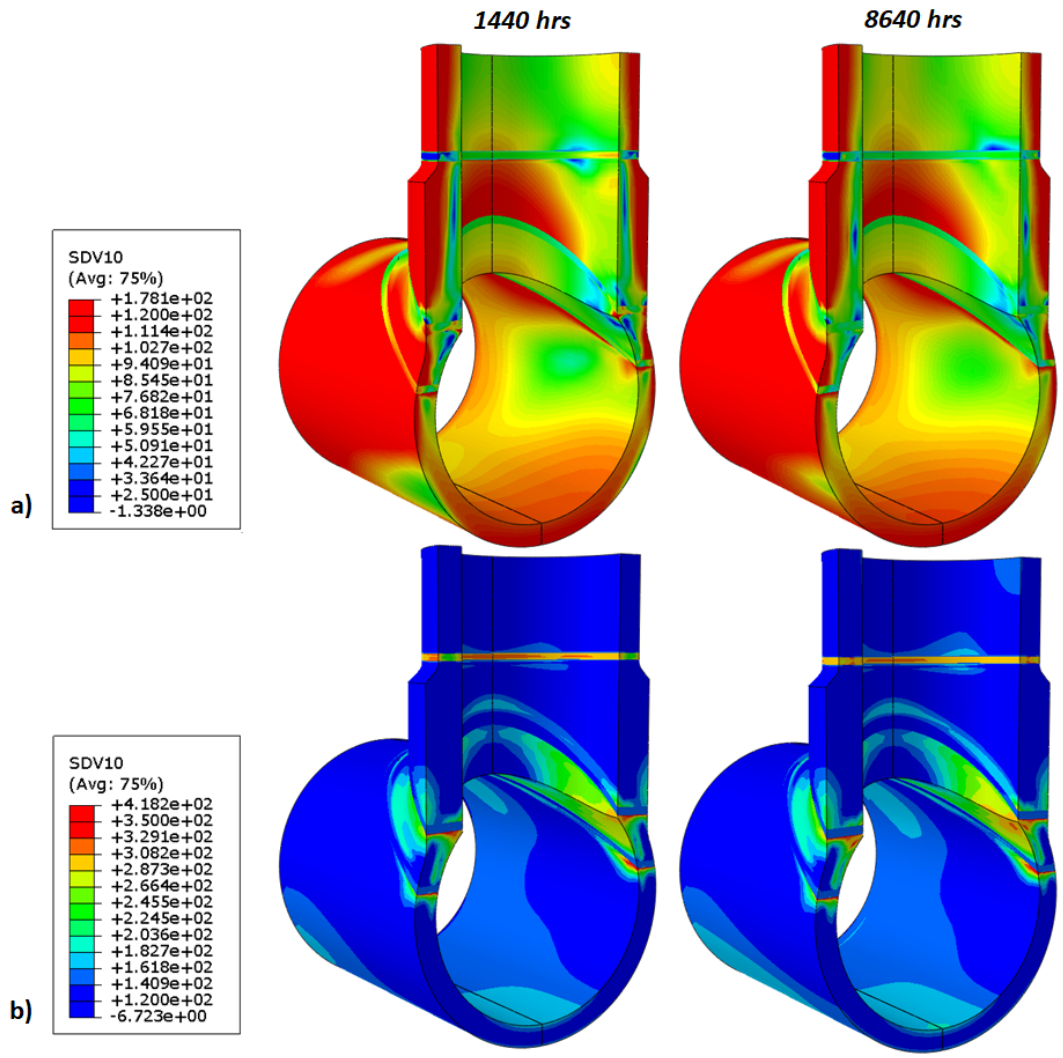

Figure 9 Stress contours for different dwell times a) end of dwell; b) unloading.

Figure 10 presents the evolution of creep strain and total strain with increasing dwell time. For all the dwell times, the plastic strain accumulation during loading is very similar. With the increase in dwell time, the creep strain increases with the area of creep strain accumulation growing from the main pipe-weldolet weldment region to the inner pipe region. The branch pipe-weldolet region shows substantial creep strain accumulation only at very high dwell times. Hence, the most critical region for creep-fatigue crack initiation is at the main pipe-weldolet weldment. Unlike the plastic strain accumulation during loading, the plastic strain accumulated during unloading increases with increasing dwell time. The stress drop which happens as a result of increasing the dwell time increases the reverse plasticity. It is to be noted that the plastic strain accumulation is highly localised.

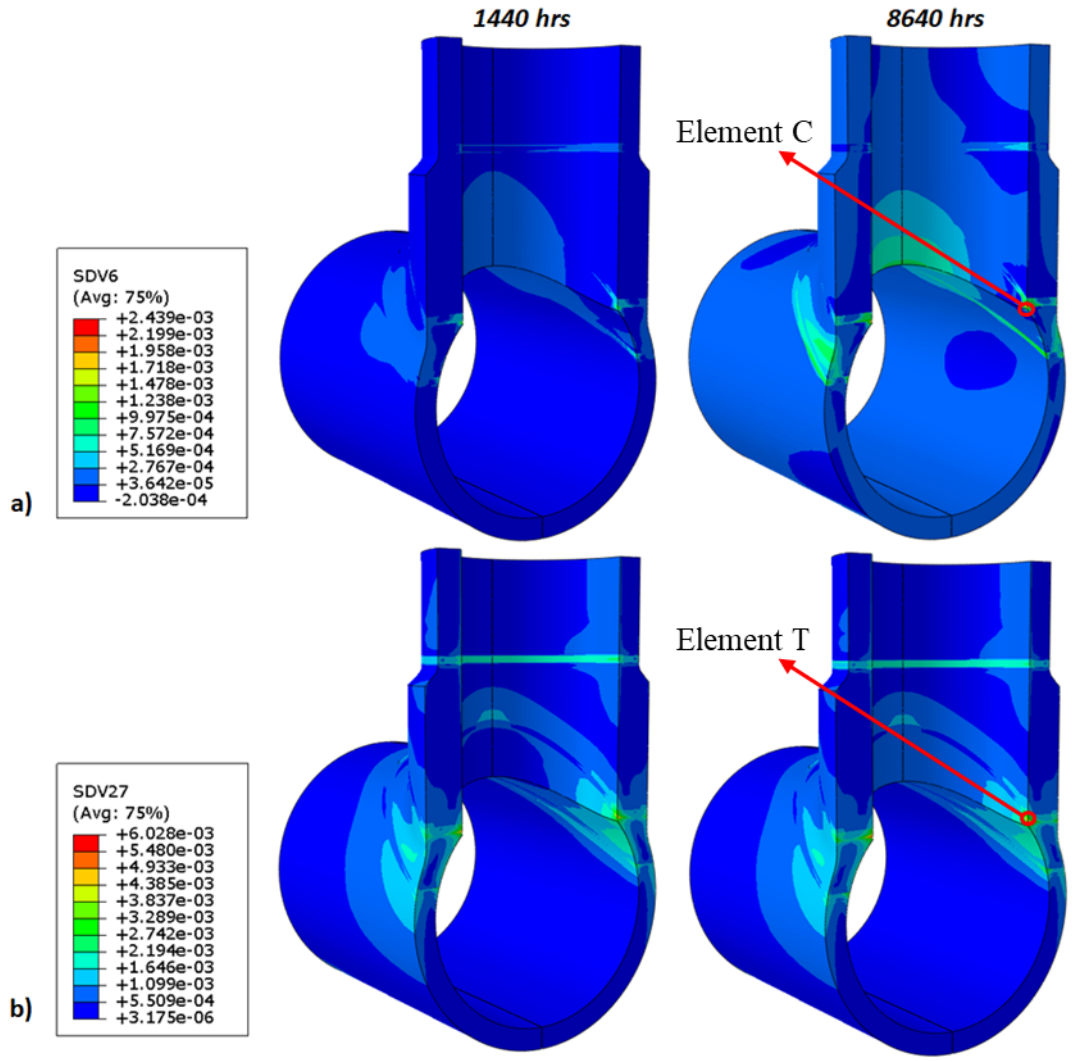

Figure 10 Effective strain contours for different dwell times a) creep; b) total strain range.

For further discussions, two of the most critical locations are identified, one where the total strain range is maximum; element - 583, within the HAZ, hereafter referred to as element T, and the other where the creep strain is maximum; element 4931, within the WM hereafter referred to as element C. For all the dwell times considered, the maximum creep strain is within the same element. It is interesting to note that this element is different from the elements that showed maximum stress concentration during the initial elastic stress analysis. The reasons for this can be better explained and discussed with the help of a hysteresis loop, which is done in the subsequent sections. Figure 11 shows the effect of various creep dwell for element T. The two most obvious effect of creep dwell on the component that can be visually inferred are that it enhances the reversed plasticity through the stress relaxation resulting in a larger hysteresis loop and the introduction of creep-ratcheting phenomena.

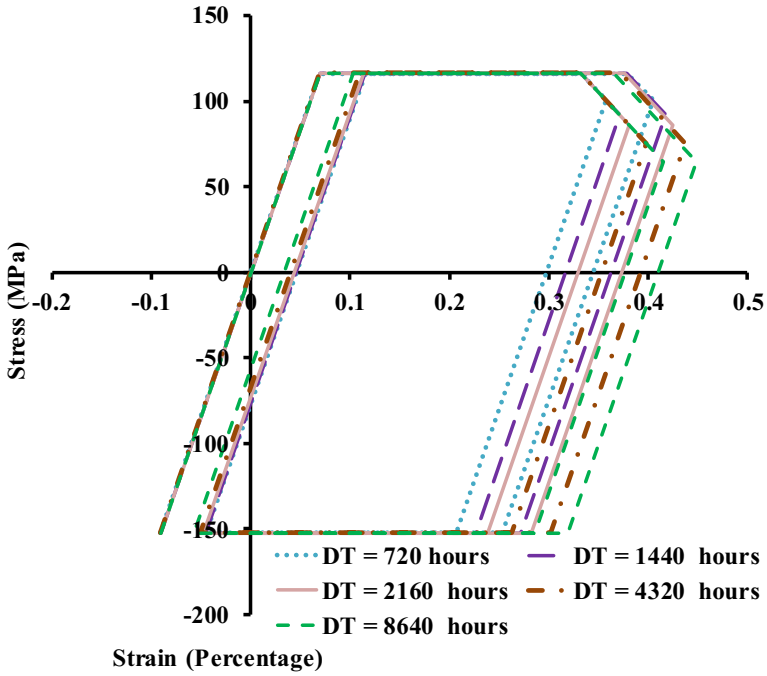

Figure 11 Steady-state hysteresis loop for increasing dwell times for element - T.

To have a deeper understanding of the effect of dwell time on the creep cyclic plasticity response of the weldolet, a plot comparing the magnitude of the loading, unloading and creep strains are presented in Figure 12 (a). It can be seen that the plastic strain magnitude during loading is nearly constant, whereas, the plastic strain magnitude during unloading increases gradually with increasing dwell times with the cross over at around dwell times of 1000 hours. The creep strain on the other hand increases in proportion to the increase in the reverse plasticity. The most significant changes occur up to a dwell time of 2000 hours after which the increase is almost linear. Nevertheless, the net plastic strain is always higher than the creep strain resulting in the creep-ratcheting mechanism. Figure 12 (b) depicts a comparison between the accumulated creep strain and net plastic strain that can be used to understand the driving factor of the creep-ratcheting process. The 45° red line indicates a closed hysteresis loop, which occurs when the net plastic strain compensates the creep strain. For lower dwell holds, the points analysed are below the closed-loop limit whereas for larger dwell times the points are above the closed limit. This indicates creep-ratcheting is driven by reverse plasticity in the former case and cyclically enhanced creep in the latter case. The above discussions highlight the effects of creep dwell time on both the shape of the hysteresis loop and the creep-cyclic plasticity response of the weldolet. Unlike the pure fatigue case, the accumulated net plastic strain is quite substantial here such that it cannot be neglected. Hence it is required that checks be performed to ascertain the creep-ratcheting damage and compare them with the creep-fatigue damage of the weldolet.

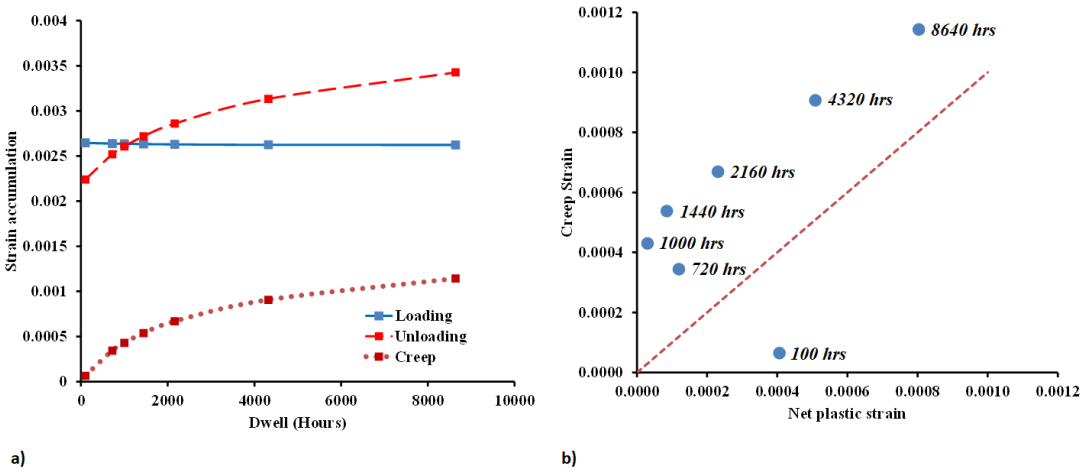

Figure 12 For element - T a) Plot comparing the magnitude of loading, unloading and creep strains; b) Creep-ratcheting interaction diagram for different dwell times.

Figure 13 presents the steady-state hysteresis loop for C. Compared to T, where an open hysterics loop is observed in the absence of creep dwell, C exhibits elastic behaviour. This is because element C is within the WM wherein the yield stress is higher than that of the HAZ and the overall stress level during loading is below the yield.

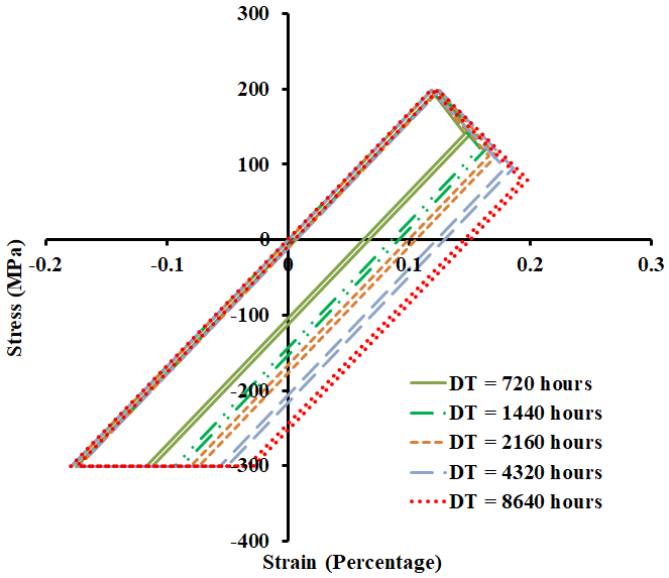

Figure 13 Steady-state hysteresis loop for increasing dwell times for element - C.

On introducing a creep dwell, the creep strain accumulates and the subsequent stress relaxation enhances the plastic behaviour during unloading. In effect, the introduction of a creep dwell induces both LCF damage as seen from the width of the hysteresis loop and creep damage as seen from the stress relaxation within this region. The plot comparing the magnitude of the unloading and creep strains for element-C are presented in Figure 14 (a). There is an exponential rise in the strain accumulation for

dwell times up to 2000 hours, after which the increase follows a linear trend. Figure 14 (b) presents the comparison of the creep strain and net plastic strain. All the points considered lie on or very close to the closed-loop limit.

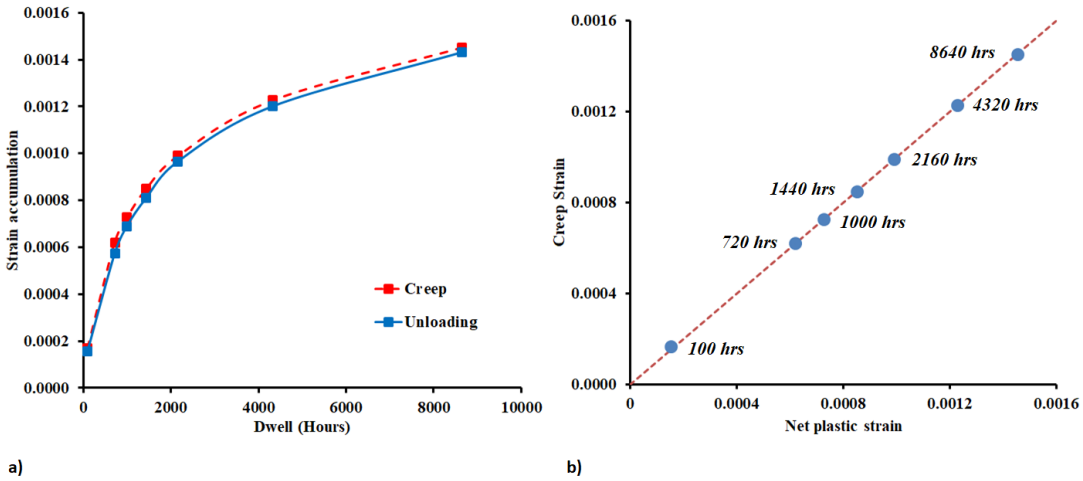

Figure 14 For element - C a) Plot comparing the magnitude of loading, unloading, and creep strains; b) Creep-ratcheting interaction diagram for different dwell times.

5.3 Creep-fatigue and creep-ratcheting damage calculations

In a single material structure, it is safe to assume that crack initiation will begin from T. But, as the component considered here is a weldment where the welding process has altered the creep and fatigue tolerance at the different zones, damage studies are required to assess the crack initiation region. Figure 15 presents the comparison between the hysteresis loop for element T and C for dwell times of 1440 hours. For element C, both the start and end of dwell stress are substantially larger than element T, this leads to higher average creep stress which will lead to a higher creep damage. On the other hand, as the width of the hysteresis loop of element T is much larger than that of element C, fatigue damage is more prominent within this region.

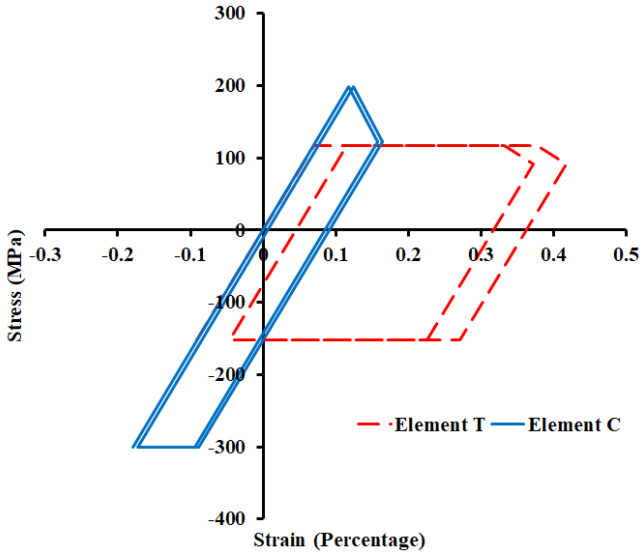

Figure 15 Hysteresis loop comparison for element T and C for dwell times of 1440 hours.

From the hysteresis loop in Figure 11 and the creep strain-net plastic strain comparison presented in Figure 12, it is clear that element T is subjected to creep ratcheting. Hence before comparing the creep-fatigue cycles to failure at element T and element C, it is necessary to analyse whether creep-ratcheting or creep-fatigue damage is more prominent at element T. Kapoor A, in [22] suggested the below formula for the evaluation of the safe life of components subjected to ratcheting

$$N_r = \frac{\varepsilon_{cr}}{\Delta\varepsilon_r} \tag{18}$$

where N_r is the number of cycles to failure by ratcheting, $\Delta\varepsilon_r$ is the ratcheting strain per cycle and ε_{cr} is the accumulated strain at which the component is considered to fail.

Figure 16 presents the comparison between the creep-fatigue life and creep-ratcheting life for dwell times up to 8640 hours. For lower dwell times, the number of cycles to failure due to creep-fatigue is much larger than cycles to failure due to creep ratcheting. On increasing the dwell time, creep-fatigue damage becomes more significant owing to the high creep damage. It is interesting to note that the creep-ratcheting damage is independent of dwell time. This is because the reverse plasticity is able to compensate for most of the inelastic strain but for a small plastic strain produced during loading which remains constant. Hence, it can be concluded that for dwell times over 720 hours creep-fatigue is the prominent damage mechanism at element T.

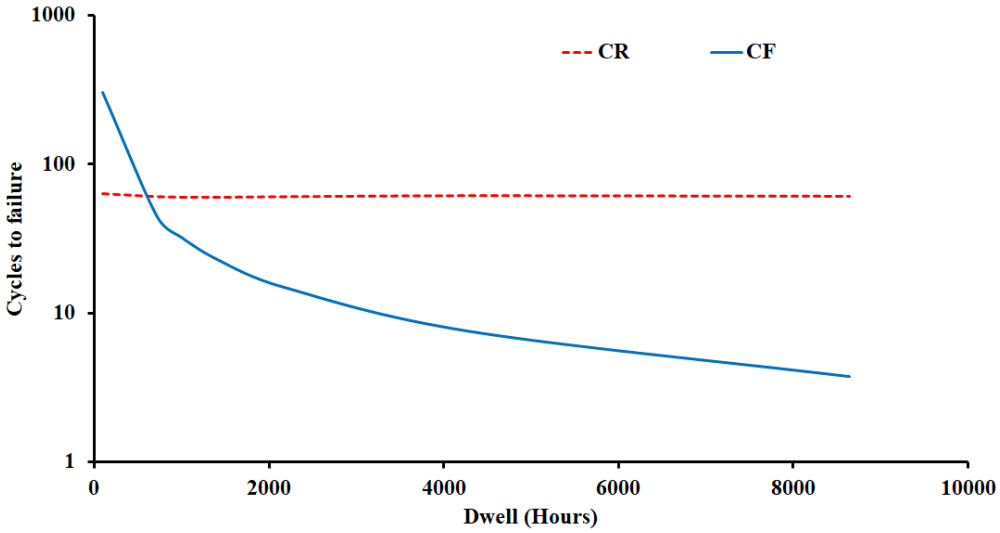

Figure 16 Comparison between creep-fatigue and creep-ratcheting life against dwell time.

Figure 17 reflects the number of cycles to failure and change in damage with increasing dwell times for both the elements. On increasing the dwell time, the cycle to failure decreases, with the decrease in the number of cycles being more prominent in element-C. For element T, though with the increase in dwell time, there is an accumulation of damage, it is not as steep as with element-C.

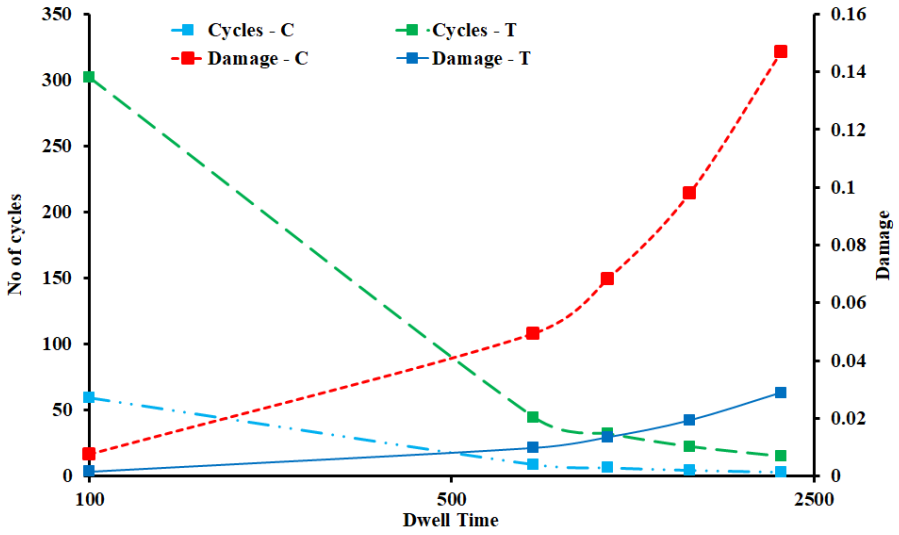

Figure 17 Total damage and cycle to failure against dwell times.

Figure 18 shows the variation of fatigue damage per cycle and creep damage per cycle with increasing dwell times. Both creep and fatigue damage increase with an increase in dwell time. But it evident that the total damage is driven by creep. The fatigue damage at element T is higher than element C for all dwell times considered while creep damage is much higher at element C compared to element T, this can be attributed to the higher average creep stress at element C coupled with the high damage constants in Equation (10) for WM.

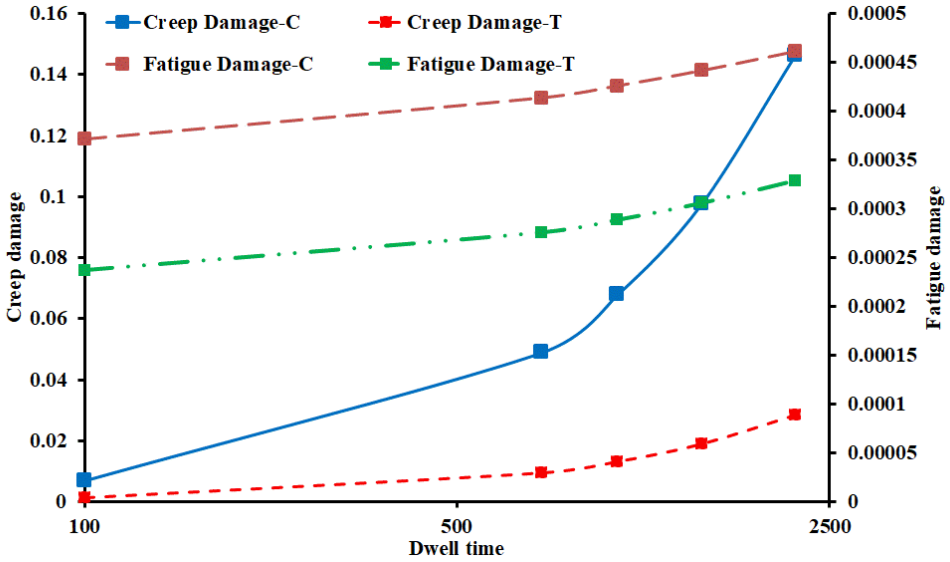

Figure 18 Creep and fatigue damage per cycle against dwell times.

The effect of a larger mechanical load is investigated for internal pressure of 25 MPa. Figure 19 presents a comparison between the hysteresis loops for both the elements T and C at a dwell time of 2160 hours. For element C, the hysteresis loop is similar indicating that the additional mechanical load has no effect whereas, for element T, a reduction in the ratchet strain accumulation is observed. This results from the lesser accumulation of plastic strain during loading, nevertheless, this is very minimal and is not expected to have any significant difference in the creep-fatigue damage life.

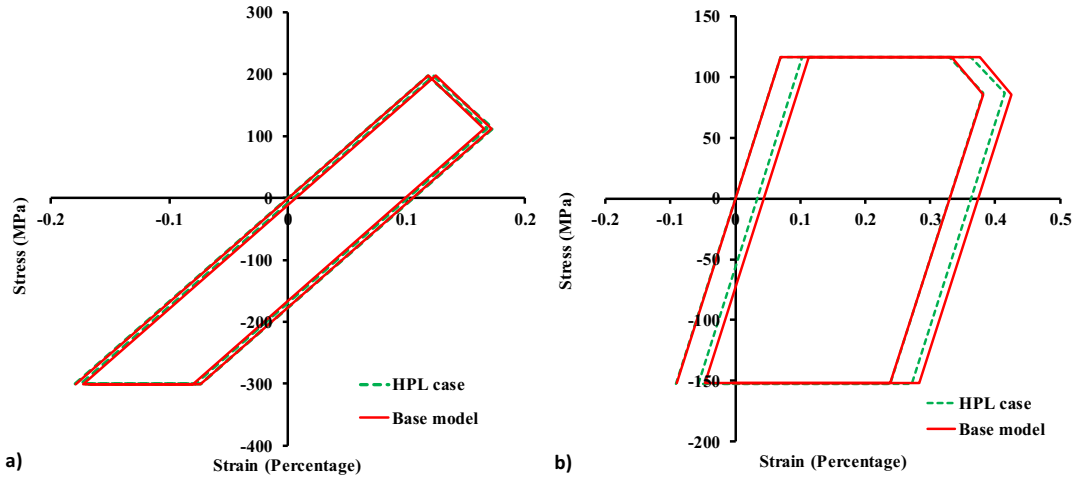

Figure 19 Steady-state hysteresis loop for High-Pressure Load (HPL) of 25 MPa and base model for DT of 2160 hours at a) element C; b) element T.

However, the increase in the mechanical load leads to very large ratchet strain accumulation towards the outer side of the weldolet at the HAZ-PM interface with the main pipe, Figure 20 (a). Figure 20 (b)

provides a comparison between the creep-fatigue life at element C and ratcheting life at the element identified with maximum ratchet strain accumulation per cycle.

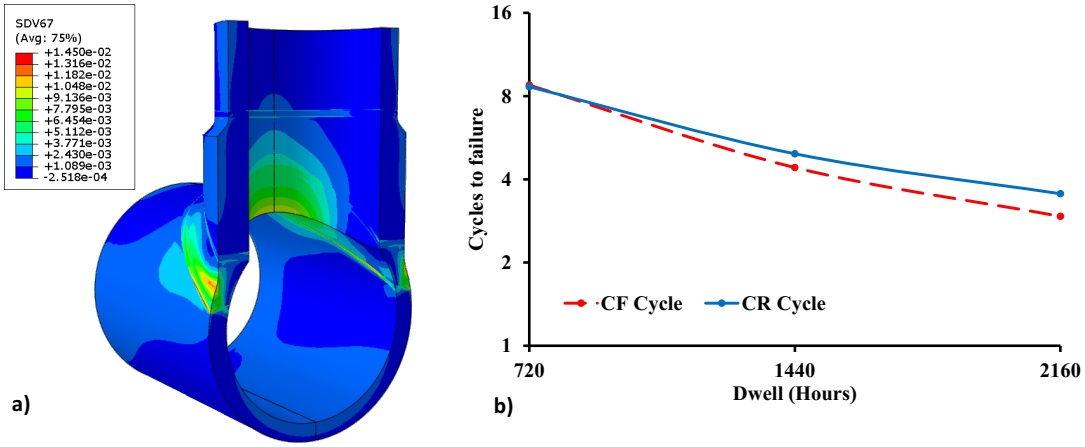

Figure 20 For larger internal pressure of 25 MPa a) Contour for ratchet strain; b) Comparison between creep-fatigue and creep-ratcheting life against dwell time.

The number of cycles to ratchet damage is very close to that to creep-fatigue damage such that the damage may initiate due to any of the mechanisms. Figure 21 presents the hysteresis loop for the element with maximum ratcheting strain. It can be observed that during creep dwell, no stress relaxation takes place within this element though large creep strain accumulation occurs.

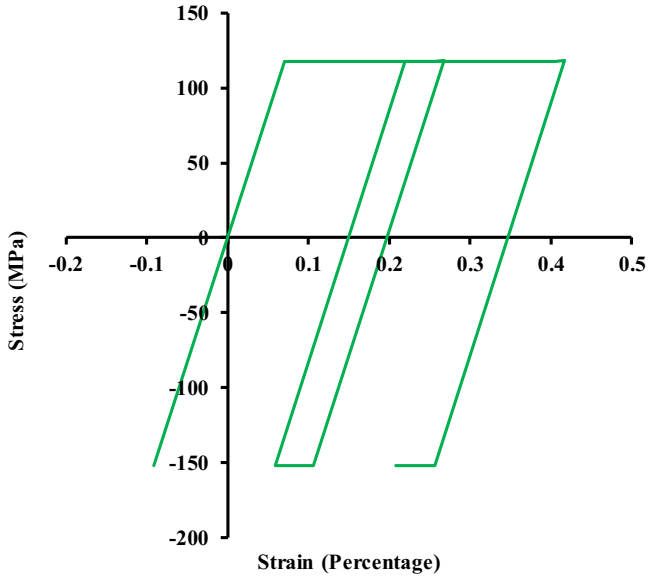

Figure 21 Steady-state hysteresis loop for HPL at the element with maximum ratcheting strain.

The effect of a thermal load is investigated by imposing an inner temperature of 740 °C, 1.2 times the initial thermal load. The analysis is restricted to a maximum dwell time of 100 hours as above this the damage is similar to that of monotonic creep rupture. Figure 22 presents the comparison of the hysteresis

loop for elements T and C for a creep dwell of 100 hours for the baseline temperature and the High-Temperature Load (HTL).

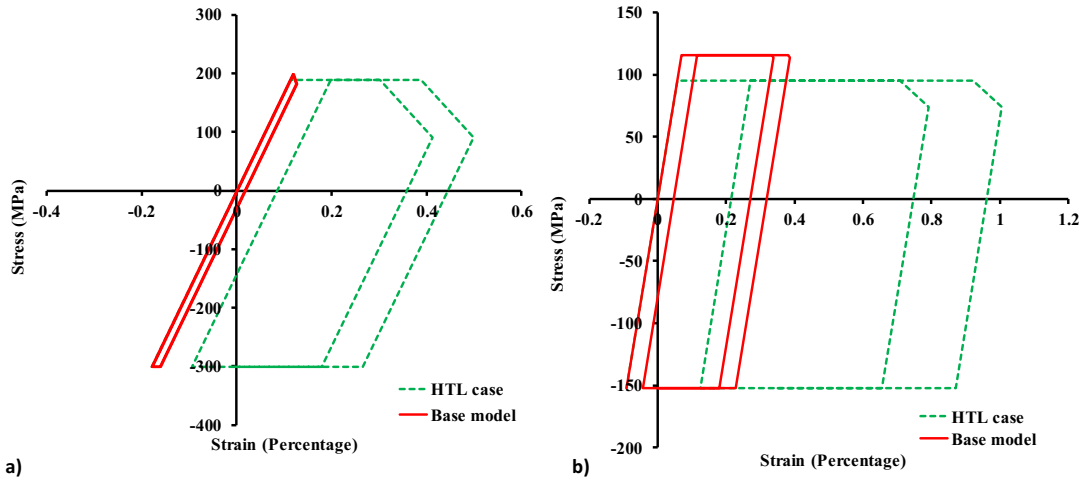

Figure 22 Steady-state hysteresis loop for High-Temperature Load (HTL) of 740 °C and base model for DT of 100 hours at a) element C; b) element T.

The plastic strain during loading is drastically enhanced by the increase in temperature. Element C which was otherwise exhibiting a closed-loop now has an open loop. One of the reasons for this is that as temperature-dependent material properties are used yielding starts at a much lower stress level. The creep strain also increases significantly for both the elements suggesting a more prominent creep-ratcheting mechanism.

6. Conclusions

Creep-cyclic plasticity interaction and life assessment of an SS304 weldolet subjected to a combined mechanical and thermal load is investigated. The structure is modelled using a quarter 3D model and temperature-dependent material properties are used for the analysis to replicate a more realistic creep-cyclic plasticity behaviour and lifetime prediction. The main observations include:

1. For the pure fatigue case, the crack is predicted to initiate after 4250 cycles but with the introduction of a creep dwell this is considerably reduced. The introduction of a creep dwell increases the total strain range. This is due to the increase in the reverse plasticity resulting from the creep relaxation. In effect this leads to the creep-fatigue interaction. For both the most critical locations identified, an increase in the dwell period led to larger stress relaxation and larger reverse plasticity.

2. Due to the different creep-cyclic plasticity behaviour and interaction of the PM, WM and HAZ, creep-fatigue damage is observed both within the WM, and the HAZ. In addition to this, creep-ratcheting damage accumulation is also observed within the HAZ. However due to the large creep parameters of the WM coupled with higher average creep stress, the creep damage within the WM is large, and the subsequent creep-fatigue interaction is expected to drive the crack initiation process. Hence, while conducting creep-fatigue damage analysis for weldments, each zone should be thoroughly investigated to identify the damage mechanism that occurs simultaneously within them.

3. All the key parameters such as the mechanical load, the thermal load and dwell period are confirmed to have a significant effect on the creep-fatigue and creep-ratcheting interactions. For thermal load dominated loading combinations, creep-ratcheting driven by reverse plasticity is observed within the HAZ for shorter dwell time. Conversely, for larger dwell times creep-ratcheting is due to cyclically enhanced creep. The larger mechanical load results in large plastic strain accumulation during loading, driving the component towards creep-ratcheting mechanism initiating from the outer side of the weldolet at the PM-HAZ interface.

Acknowledgments

The authors gratefully acknowledge the supports from the National Natural Science Foundation of China (51828501) and the University of Strathclyde during the course of this work.

References

[1] T. Asayama, “Creep-fatigue evaluation of stainless steel welded joints in FBR class 1 components,” *Nucl. Eng. Des.*, vol. 198, no. 1, pp. 25–40, 2000.

[2] T. A. S. of Mechanical Engineers, “Section III, Division 1, Subsection NH, Class 1 Components in Elevated Temperature Service,” *Am. Soc. Mech. Eng.*, 2014.

[3] Ainsworth, R., "R5: Assessment procedure for the high temperature response of structures," *British energy generation Ltd*, 2003

[4] Y. Yang and W. C. Mohr, “Weld residual stress and creep-fatigue analysis of a furnace roll in a continuous hot dip coating line,” *Proc. ASME 2016 Press. Vessel. Pip. Conf.*, vol. Volume 6B:, no. Vancouver, British Columbia, Canada. July 17–21, 2016. V06BT06A074. ASME., 2016.

[5] N. Cho, “Structural integrity assessment of engineering components under cyclic loading at high temperature,” *PhD Thesis, Univ. Strat.*, 2019.

[6] D. Barbera, “On the evaluation of high temperature creep-fatigue responses of structures,” *PhD*

Thesis, Univ. Strat., 2017.

[7] H. Chen, W. Chen, and J. Ure, "A direct method on the evaluation of cyclic steady state of structures with creep effect," *J. Press. Vessel Technol.*, vol. 136, no. 6, p. 061404, 2014.

[8] D. Barbera, H. Chen, and Y. Liu, "On creep fatigue interaction of components at elevated temperature," *J. Press. Vessel Technol.*, vol. 138, no. 4, p. 041403, 2016.

[9] M. Puliyaneth, H. Chen, and W. Luan, "Creep fatigue damage assessment of V-butt weld pipe with an extended direct steady cycle analysis," *Am. Soc. Mech. Eng. Press. Vessel. Pip. Div. PVP*, vol. 5, pp. 1–9, 2018.

[10] H. F. Chen and A. R. S. Ponter, "Shakedown and limit analyses for 3-D structures using the linear matching method," *Int. J. Press. Vessel. Pip.*, vol. 78, no. 6, pp. 443–451, 2001.

[11] H. Chen, "Lower and upper bound shakedown analysis of structures with temperature-dependent yield stress," *J. Press. Vessel Technol.*, vol. 132, no. 1, p. 011202, 2010.

[12] J. Ure, H. Chen, T. Li, W. Chen, D. Tipping, and D. Mackenzie, "A direct method for the evaluation of lower and upper bound ratchet limits," *Procedia Eng.*, vol. 10, pp. 356–361, 2011.

[13] A. R. S. Ponter and H. Chen, "A minimum theorem for cyclic load in excess of shakedown, with application to the evaluation of a ratchet limit," *Eur. J. Mech. A/Solids*, vol. 20, no. 4, pp. 539–553, 2001.

[14] Y. Gorash and H. Chen, "Creep-fatigue life assessment of cruciform weldments using the linear matching method," *Int. J. Press. Vessel. Pip.*, vol. 104, pp. 1–13, 2013.

[15] H. Chen and A. R. S. Ponter, "Linear matching method on the evaluation of plastic and creep behaviours for bodies subjected to cyclic thermal and mechanical loading," *Int. J. Numer. Methods Eng.*, vol. 68, no. 1, pp. 13–32, 2006.

[16] R. P. Skelton and D. Gandy, "Creep-fatigue damage accumulation and interaction diagram based on metallographic interpretation of mechanisms," *Mater. High Temp.*, vol. 25, no. 1, pp. 27–54, 2008.

[17] S. B. Leen, R. A. Barrett, D. Joyce, M. Li, S. Scully, and P. E. O'Donoghue, "High temperature, multi-material, cyclic plasticity of a P91 welded branch-header connection under cyclic pressure," *Am. Soc. Mech. Eng. Press. Vessel. Pip. Div. PVP*, vol. 3, July, 2015.

[18] M. Li, R. A. Barrett, S. Scully, N. M. Harrison, S. B. Leen, and P. E. O'Donoghue, "Cyclic plasticity of welded P91 material for simple and complex power plant connections," *Int. J. Fatigue*, vol. 87, pp. 391–404, 2016.

[19] D. Hibbitt, B. Karlsson and P. Sorensen, "Abaqus 6.12. 3 manual," 2012.

[20] A. Hossein, D. Sorkhabi, and F. Vakili-tahami, "Experimental study of the creep behavior of parent, simulated HAZ and weld materials for cold-drawn 304L stainless steel," *Eng. Fail. Anal.*, vol. 21, pp. 78–90, 2012.

[21] A. Sorkhabi and F. V. Tahami, "Creep constitutive equation for 2- materials of weldment-304L stainless steel," *Int. J. Mech Mechatronics*, vol. 6, no. 1, 2012.

[22] A. Kapoor, “a Re-Evaluation of the Life To Rupture of Ductile Metals By Cyclic Plastic Strain,” *Fatigue Fract. Eng. Mater. Struct.*, vol. 17, no. 2, pp. 201–219, 1994.